Available online at www.sciencedirect.com
ScienceDirect
Journal of the European Ceramic Society 29 (2009) 2823–2830
www.elsevier.com/locate/jeurceramsoc

Chemical compatibility of proton conducting $LaNbO_4$ electrolyte with potential oxide cathodes

J.R. Tolchard, H. Lea Lein, T. Grande *

Department of Materials Science and Engineering, Norwegian University of Science and Technology, N-7491 Trondheim, Norway

Received 28 January 2009; received in revised form 25 March 2009; accepted 31 March 2009
Available online 17 May 2009

Abstract

The chemical and physical compatibility of the proton conducting electrolyte material $LaNbO_4$ with the potential partner materials $LaMO_3$ (M=Mn, Fe, Co) and La_2NiO_4 is investigated via the reaction of fine-grained powders and solid-state diffusion couples. Results show generally good chemical compatibility for $LaNbO_4$ with perovskite type compositions, particularly the $LaFeO_3$ and $LaMnO_3$ systems. In contrast, Ruddlesden–Popper type phases are predicted to be poor candidates for use with $LaNbO_4$. Investigation of the La_2O_3–NiO–Nb_2O_5 and La_2O_3–CoO–Nb_2O_5 phase diagrams finds two new perovskite-related materials of stoichiometry $LaNb_{1/3}M_{2/3}O_3$ (M=Ni, Co), and indicates coexistence of $LaNbO_4$ with the binary oxides NiO and CoO. Additionally, reduction of a $LaNbO_4$–NiO composite confirms coexistence of $LaNbO_4$ with Ni, and so it is concluded that doped-$LaMO_3$|$LaNbO_4$|Ni-$LaNbO_4$ type electrochemical cells may be manufactured via a direct co-firing route without the formation of secondary phases at inter-phase boundaries.

Keywords: SOFC; $LaNbO_4$; Proton conducting electrolyte; Materials compatibility; Perovskite

1. Introduction

Hydrogen is an important industrial feedstock used in large quantities by the petro- and agro-chemical industries. Additionally it is forecast to become a key part of the next generation power production and distribution infrastructure, provided new technologies for the efficient large-scale production and utilisation of H_2 can be developed. Central to these technologies is the development of improved ionically conducting membranes, as they form the core of devices such as steam electrolysers, hydrogen separators and fuel cells which are expected to underpin the forthcoming hydrogen economy.

Such membranes typically conduct either protons, oxide or hydroxide ions, and may operate between room temperature and 1000 °C depending on application. High temperature systems based on ceramic oxides are increasingly being viewed as attractive options for static applications owing to their high efficiency and greater tolerance for fuel impurities. To date, such systems have tended to be based around an oxide ion conducting membrane operating close to 1000 °C, but lower temperature is extremely attractive as it improves device lifetime and reduces manufacturing costs. This has focussed attention on proton conducting ceramics. State of the art in this respect are the perovskite structured alkaline earth cerate and zirconate systems,[1–4] which offer high performance at intermediate temperatures, but suffer from poor chemical and mechanical stability under typical operational conditions.[5] Their application is also hindered by the processing difficulties associated with H_2O and CO_2 uptake at intermediate temperatures,[6] and for the zirconates, poor sinterability.[7]

Recently a new family of *ortho*-niobate proton conductors was reported by Haugsrud and Norby.[8] Whilst these do not offer the performance of the best cerate and zirconate systems (~0.001 S cm^{-1} at 950 °C for Ca-doped $LaNbO_4$),[9] considerably reduced reactivity with respect to both water and CO_2. This translates into both easier materials processing and improved stability under "real world" operating conditions, making them attractive for applications such as solid oxide fuel cells (SOFCs) where long term stability under humid/CO_2 atmospheres is crucial. However, application of these materials requires appropriate electrode partner materials need to be found. Ideally a material exhibiting high levels of protonic and electronic con-

* Corresponding author.
E-mail address: tor.grande@material.ntnu.no (T. Grande).

0955-2219/$ – see front matter © 2009 Elsevier Ltd. All rights reserved.
doi:10.1016/j.jeurceramsoc.2009.03.034

ductivity, appropriate catalytic activity and thermal and chemical compatibility with the electrolyte material is desired. Unfortunately all of these objectives have yet to be realised in an oxide form, and so in protonic systems it is common to implement a metallic or electrolyte cermet anode (usually using nickel)[10,11] and a platinum/noble metal cathode.[12] It has recently been proposed that the use of a mixed electronic and oxide conducting cathode,[13] possibly in the form of a composite with the electrolyte material, would offer a degree of tailorability absent when noble metals are used, and would reduce raw material costs. Many of these materials also have the advantage of being relatively mature technologies. Accordingly, we have chosen to evaluate the chemical compatibility of $LaNbO_4$ with the model materials, $LaMO_3$ (M=Mn, Fe and Co) and La_2NiO_4. $LaMO_3$ (M=Mn, Fe and Co) substituted with alkali earth on the lanthanum site are prime candidates as cathode materials (Sr-substituted $LaMnO_3$ is the state of the art cathode in SOFC). Materials with alkali earth substitution were however not used in this study to reduce the number of chemical components and to simplify the investigation. The chosen systems are intended to reflect the wider oxide cathode systems, with the results providing a basis for prediction of likely candidates beyond those tested.

2. Experimental

Powders of $LaMnO_3$, $LaFeO_3$, $LaCoO_3$ and La_2NiO_4 were synthesised via spray pyrolysis of appropriate solutions of metal nitrates. A complexing agent, ethylenediaminetetraacetic acid (EDTA), was used to assist dissolution and homogeneous reaction during pyrolysis. Synthesis of $LaNbO_4$ was via a more complex route using a Nb-malic precursor and is reported in detail elsewhere.[14] As-prepared powders were then calcined in air at 800–900 °C to remove residual nitrates/organics, and milled in isopropanol for 6–8 h using 5 mm zirconia media. The resulting final product was a pure, finely divided, sub-micron powder.

To assess phase compatibility with $LaMO_3$ (M=Mn, Fe, Co), 1:1 mixtures (by mass) of $LaNbO_4$:$LaMO_3$ were ground together, pressed into tablet form and fired at 1150 °C in 36 h segments, with a regrinding step between each. Reaction of $LaNbO_4$ with La_2NiO_4 was ascertained for three composition ratios: 1:1, 1:2 and 2:1, measured again by mass. In the wider La_2O_3–NiO–Nb_2O_5 phase diagram, dried powders of high quality commercially produced binary oxides were used, again being reacted in tablet form. Stability under reducing conditions was assessed via reaction at 900 °C under a flowing atmosphere of 5% H_2 in N_2.

Additionally, dense $LaNbO_4$ ceramics were produced via uniaxial compression at 80 MPa, followed by firing at 1200 °C for 6 h in air. These were then polished with fine abrasives down to 1 μm and a slurry of $LaMO_3$ (M=Mn, Fe) coated on the surface to form a diffusion couple. The couples thus formed were fired at 1300 °C for 36 h, with heating and cooling rates of 200 °C/h.

Phase formation in the powder samples was analysed using a Bruker D8 Advance powder diffractometer (Cu-Kα radiation, Våntec detector). Phases were identified via the PDF database, with Rietveld refinement and profile fitting performed using the Topas 2.1 software suite. The microstructure of diffusion couples was studied using an Hitachi N-3400 scanning electron microscope (SEM) equipped with an Oxford Instruments INCA X-sight (model 7021) energy dispersive X-ray spectroscopy spectrometer (EDS). Samples for SEM/EDS analysis were mounted in epoxy resin, polished with fine abrasives (down to 1 μm) and coated with carbon. Sample compositions were analysed via both spot analyses and X-ray element mapping, with line profiles calculated from the element maps using a spot size in the region 9–16 μm^2. All analysis was performed using the Oxford Instruments INCA analysis tools, calibrated relative to a Co standard, with the estimated error in cation compositions being <5%.

3. Results

Mixtures of microfine powders of $LaNbO_4$ with $LaMO_3$ (M=Mn, Fe and Co) were initially fired for between 72 and 144 h with diffractograms collected at 36 h intervals. For M=Mn and Fe, no secondary phases were observed after the initial firing step, but the powders were subjected to further firing to determine the extent of any interdiffusion which may occur. For both $LaCoO_3$ and La_2NiO_4, reaction with $LaNbO_4$ was observed, with equilibrium being obtained after the third firing step (108 h total firing time). We note that for all systems the presence of two phases at equilibrium is in good accord with the Gibbs phase rule, $ph + f = c + 2$, where c is the number of components (La + Nb + M + O = 4), f is the number of degrees of freedom, and ph is the number of phases present.

Diffractograms of the M=Mn and Fe systems, obtained after 72 h reaction at 1150 °C, are presented in Fig. 1 with corre-

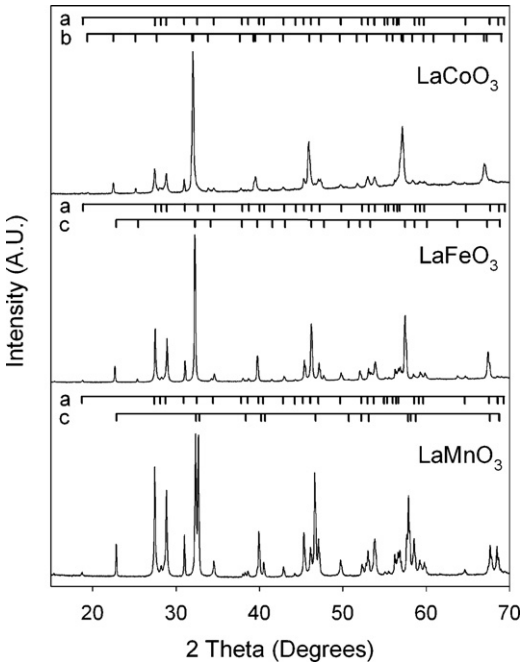

Fig. 1. X-ray powder diffractograms for powder composites of $LaNbO_4$ and $LaMO_3$ after 72 h firing at 1100 °C. Peak positions are shown for the equilibrium phases: (a) $LaNbO_4$, (b) $LaCo_{2/3}Nb_{1/3}O_3$ and (c) $LaMO_3$.

Table 1
Rietveld refinement results for powder composites of $LaNbO_4$ with $LaMO_3$ (M=Mn, Fe and Co).

Cathode system	Rwp	Phase	Space group	Unit cell	Phase fraction (wt. %)	Reference
$LaMnO_3$	5.67	$LaMnO_3$	*R*-3*c*	$a = 5.53072(6)$ $c = 13.3434(2)$	48.6(49)	30
		$LaNbO_4$	*C*2/*c*	$a = 7.3421(2)$ $b = 11.5219(4)$ $c = 5.2016(2)$ $\beta = 130.921(2)$	51.4(49)	31
$LaFeO_3$	4.86	$LaFeO_3$	*Pbnm*	$a = 5.5619(6)$ $b = 5.5538(5)$ $c = 7.8496(8)$	49.2(2)	32
		$LaNbO_4$	*C*2/*c*	$a = 7.3419(7)$ $b = 11.5206(11)$ $c = 5.2018(5)$ $\beta = 130.926(2)$	50.8(2)	31
$LaCoO_3$	3.53	$LaCo_{2/3}Nb_{1/3}O_3$	*P*21/*n*	$a = 5.5722(10)$ $b = 5.6048(11)$ $c = 7.8865(16)$ $\beta = 90.007(34)$	65.5(13)	15
		$LaNbO_4$	*C*2/*c*	$a = 7.3445(15)$ $b = 11.5327(24)$ $c = 5.2047(11)$ $\beta = 131.035(6)$	34.5(13)	31

Table 2
Rietveld refinement results for reactions occurring in the phase diagram La_2O_3–Nb_2O_5–NiO.

Ratio $LaNbO_4$:La_2NiO_4	Rwp	Phase	Space group	Unit cell	Weight fraction	Reference
1:2	3.05	La_2NiO_4	*Fmmm*	$a = 5.4540(3)$ $b = 5.4629(3)$ $c = 12.6833(6)$	16.2(1)	33
		La_3NbO_7	*Pnma*	$a = 7.7487(4)$ $b = 11.1519(6)$ $c = 7.6289(4)$	39.0(1)	34
		$LaNi_{2/3}Nb_{1/3}O_3$	*P*21/*n*	$a = 5.5812(3)$ $b = 5.6241(3)$ $c = 7.9011(5)$ $\beta = 90.001(3)$	44.8(1)	15
1:1	3.71	$LaNbO_4$	*C*2/*c*	$a = 7.3465(8)$ $b = 11.5325(13)$ $c = 5.2041(7)$ $\beta = 130.999(7)$	15.6(2)	31
		La_3NbO_7	*Pnma*	$a = 7.7503(4)$ $b = 11.1595(6)$ $c = 7.6254(4)$	39.6(2)	34
		$LaNi_{2/3}Nb_{1/3}O_3$	*P*21/*n*	$a = 5.5880(3)$ $b = 5.6375(3)$ $c = 7.9161(4)$ $\beta = 89.991(3)$	44.8(2)	15
2:1	4.92	$LaNbO_4$	*C*2/*c*	$a = 7.3426(10)$ $b = 11.5249(16)$ $c = 5.2019(7)$ $\beta = 130.939(3)$	43.8(1)	31
		La_3NbO_7	*Pnma*	$a = 7.7492(11)$ $b = 11.1538(15)$ $c = 7.6259(10)$	26.1(8)	34
		$LaNi_{2/3}Nb_{1/3}O_3$	*P*21/*n*	$a = 5.5866(9)$ $b = 5.6343(9)$ $c = 7.9125(13)$ $\beta = 89.888(12)$	30.2(2)	15

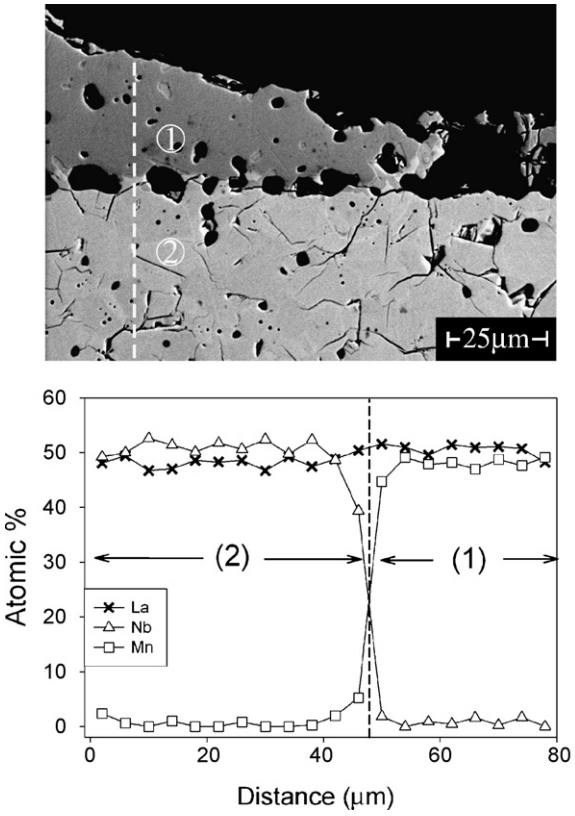

Fig. 2. (a) Backscattered electron micrograph of the $LaNbO_4/LaMnO_3$ diffusion couple following 36 h firing at 1300 °C in air. (b) Phase composition taken along the marked line in (a). The numbered regions correspond to those marked in (a).

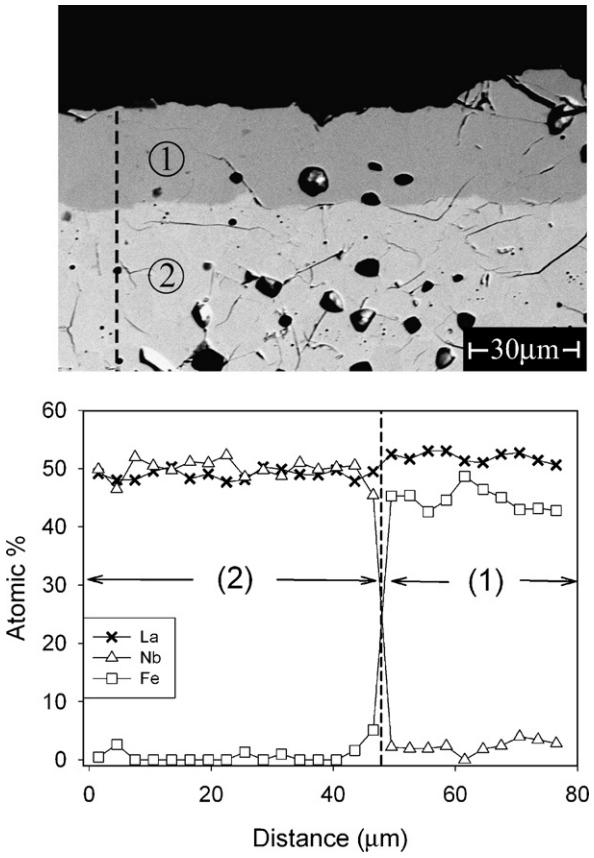

Fig. 3. (a) Backscattered electron micrograph of the $LaNbO_4/LaFeO_3$ diffusion couple following 36 h firing at 1300 °C in air. (b) Phase composition taken along the marked line in (a). The numbered regions correspond to those marked in (a).

sponding Rietveld refinement results given in Table 1. It can be seen that for the $LaNbO_4$–$LaFeO_3/LaMnO_3$ systems, no reaction is observed: No secondary phases are observed, and unit cell parameters for both $LaNbO_4$ and $LaMO_3$ phases agree excellently with literature values, indicating that no significant interdiffusion has occurred. The calculated final phase fractions also correlate with the starting phase fractions. Diffusion couples of these systems (Figs. 2a and 3a), fired at the slightly higher temperature of 1300 °C, confirm this finding, with EDS compositional analysis (Figs. 2b and 3b) showing a clear phase boundary and no evidence of diffusion of either Mn/Fe or Nb between the phases. We note that no thermodynamic barrier exists for interdiffusion of La between coexistent phases, but this cannot be measured by the techniques employed here.

Diffractograms of powder mixtures of $LaNbO_4$ with $LaCoO_3$ and La_2NiO_4 are shown respectively in Figs. 1 and 4, with Rietveld refinement results presented in Tables 1 and 2. Reaction equilibrium in both systems was observed after 144 h total firing at 1150 °C, with EDS analysis identifying the primary product phases as being of approximate composition $LaNb_{1/3}M_{2/3}O_3$. Provisional indexing of the diffractograms suggests the phases to be distorted, cation ordered perovskite of structure similar to $LaNb_{1/3}Mg_{2/3}O_3$.[15] We note that a full structural analysis of single phase samples of these materials is underway, the results of which will be reported elsewhere. For this work the $LaNb_{1/3}Mg_{2/3}O_3$ structural model[15] was applied in the multiphase Rietveld analysis of the system, allowing calculation

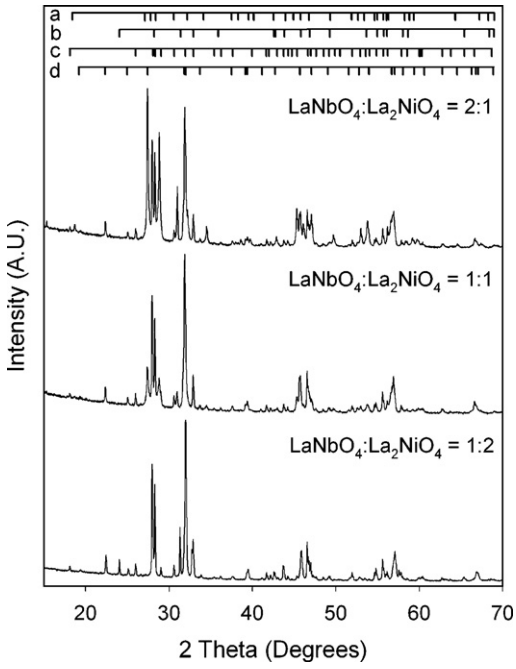

Fig. 4. X-ray powder diffractograms for powder composites of $LaNbO_4$ and La_2NiO_4 after 72 h firing at 1100 °C. The respective ratios 1:2, 1:1 and 2:1 of $LaNbO_4$:La_2NiO_4 correspond to compositions 1–3 in Fig. 5. Peak positions are shown for the equilibrium phases: (a) $LaNbO_4$, (b) La_2NiO_4, (c) La_3NbO_7 and (d) $LaNi_{2/3}Nb_{1/3}O_3$.

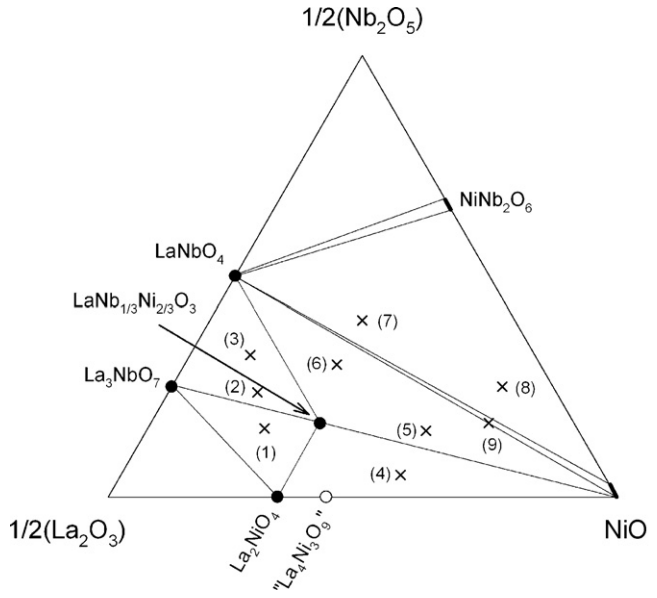

Fig. 5. Isothermal and iosobaric section of the La_2O_3–NiO–Nb_2O_5 phase diagram at 1150 °C. Alkemade lines are shown as solid lines, with solid solutions in bold. Numbers correspond to the synthesised compositions marked with an "×", and are discussed in the text. The phase "$La_4Ni_3O_9$" is projection of the oxidised phase $La_4Ni_3O_{10-\delta}$ onto the isobaric plane.

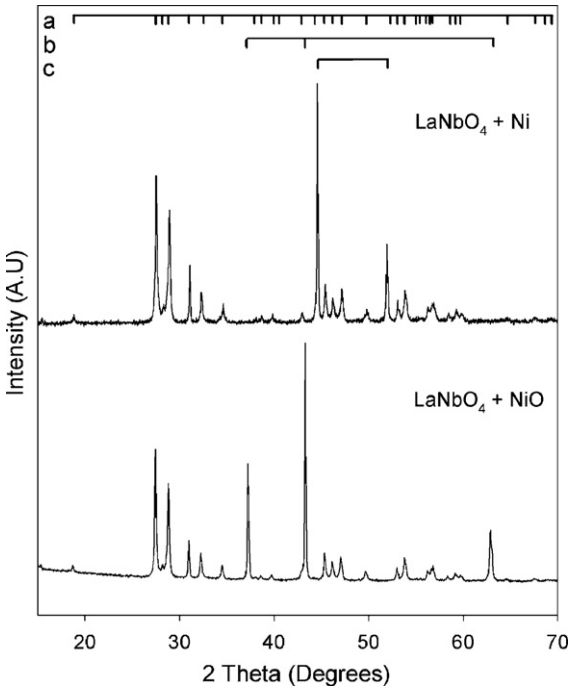

Fig. 6. X-ray powder diffractograms for the composition "9" shown in Fig. 5, before and after reduction in flowing 5% H_2 in N_2.

of the respective fractions of the product phases formed, and thus providing insight into the reactions occurring. Accordingly, for the M=Co system, relative equilibrium phase fractions of 2:1 ($LaNb_{1/3}Co_{2/3}O_3$: $LaNbO_4$) suggest the following balanced reaction:

$$2LaCoO_3 + LaNbO_4 \rightarrow 3LaNb_{1/3}Co_{2/3}O_3 + 0.5O_{2(g)} \quad (1)$$

The La_2NiO_4 system is complicated slightly by being in a more La-rich region of the respective phase diagram. Consequently a quantity of an additional phase, La_3NbO_7 is observed. In this case, the equilibrium reaction products of three compositions 1:2, 1:1 and 2:1 of $LaNbO_4$:La_2NiO_4 (labelled 1–3 in Fig. 5) were used to calculate the balanced reaction:

$$2La_2NiO_4 + 2LaNbO_4 \rightarrow 3LaNb_{1/3}Ni_{2/3}O_3 + La_3NbO_7 \quad (2)$$

The formation of the previously unreported $LaNb_{1/3}Ni_{2/3}O_3$ phase prompted a wider investigation of this portion of the ternary La_2O_3–NiO–Nb_2O_5 phase diagram. Accordingly a number of additional samples were synthesised and fired under the same conditions as the initial $LaNbO_4$/La_2NiO_4 powder compacts. Equilibrium products were identified via the PDF database[16] and confirmed via multiphase Rietveld refinement. Combination with existing data for the binary joins[17–19] allowed derivation of an isobaric–isothermal section of the ternary phase diagram La_2O_3–NiO–Nb_2O_5. This is presented in Fig. 5, with the synthesised compositions labelled 1–8. We note that as this work is concerned primarily with the compatibility of $LaNbO_4$ with potential electrode partner materials, the Nb-rich portion of the phase diagram was not explored. According to the Gibbs phase rule, a system with 4 components can show a maximum of 6 phases at equilibrium. Fixing the independent variables of temperature and pressure this reduces to 4, which accords well with our observations of three condensed phases for the system. For the composition labelled "4", a Ruddlesden–Popper phase, probably $La_4Ni_3O_{10-\delta}$,[20] was observed and as this lies out of the plane of the phase diagram presented in Fig. 5 (being partially oxidised) it has been projected onto the diagram as $La_4Ni_3O_9$.

The portion of the phase diagram investigated is relatively uncomplicated, with only one new phase found: $LaNb_{0.33}Ni_{0.66}O_3$. Coexistence of this phase with $LaNbO_4$, La_3NbO_7, La_2NiO_4 and NiO is predicted in this T–pO_2 region, though our diffraction analysis is inconclusive with respect to the limited solid solubility of Nb_2O_5 into NiO reported previously.[17] The nickel-rich niobate $Ni_4Nb_2O_9$ is not observed to form at the temperatures used here, which accords with previous studies,[21] and so an alkemade triangle linking $LaNbO_4$, $NiNb_2O_6$ and NiO is observed. This region of the phase diagram is predicted to change with the formation of $Ni_4Nb_2O_9$ at ∼1200–1250 °C.[21] A second firing of the sample labelled "9" under reducing conditions (5% H_2 in N_2) confirmed coexistence of $LaNbO_4$ with Ni also (Fig. 6), with SEM and EDS analysis (Fig. 7) respectively confirming good microstructural properties and the absence of interdiffusion between the $LaNbO_4$ and Ni phases. Accordingly, with consideration of the Ni–O binary phase diagram[22] a further alkemade triangle linking $LaNbO_4$, NiO and Ni can be predicted lying out of the plane of Fig. 5.

4. Discussion

It is clear from our results that $LaNbO_4$ shows good stability with respect to $LaMO_3$ perovskite compositions: For M=Mn/Fe no reaction is seen and for M=Co/Ni the reaction products are the perovskite materials $LaNb_{1/3}M_{2/3}O_3$. It is shown directly for the Ni system, and expected for the other systems, that the promising

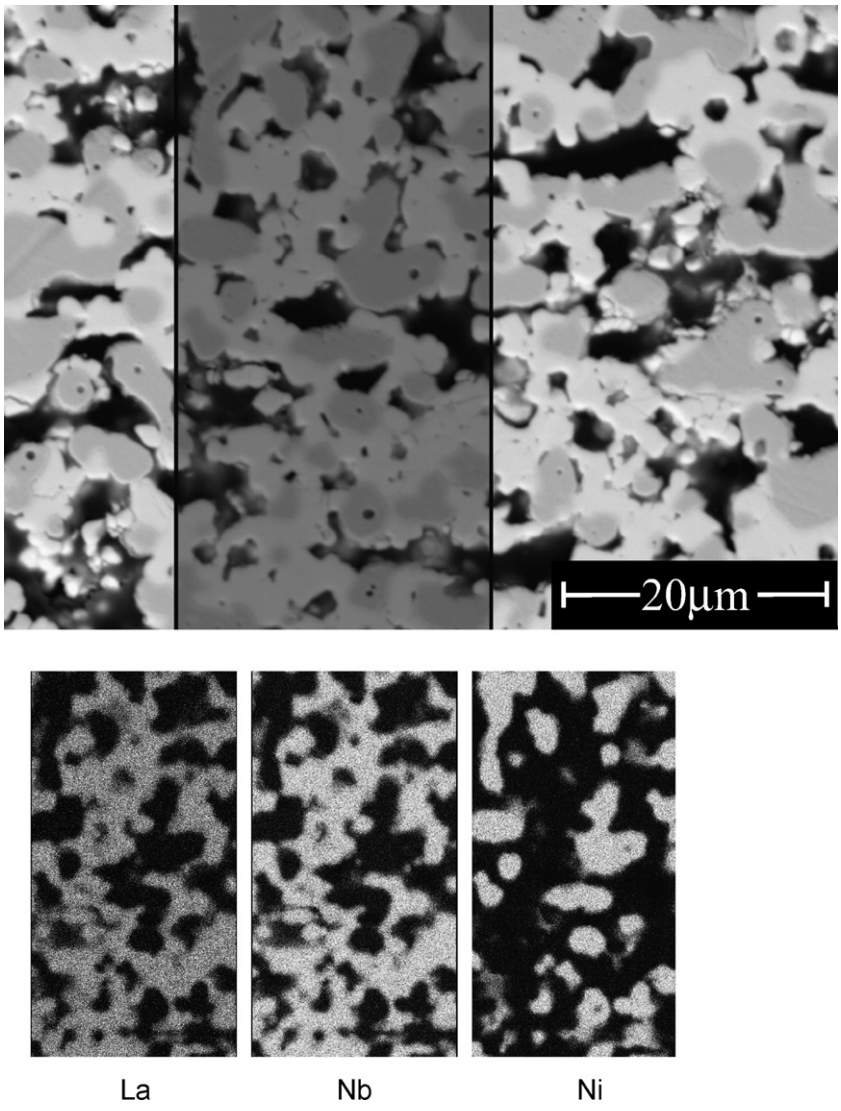

Fig. 7. (a) Backscattered electron micrograph of a $LaNbO_4$–Ni cermet formed via reduction of sample "9" in flowing 5% H_2 in N_2. (b) EDS element maps collected over the shaded area shown in (a).

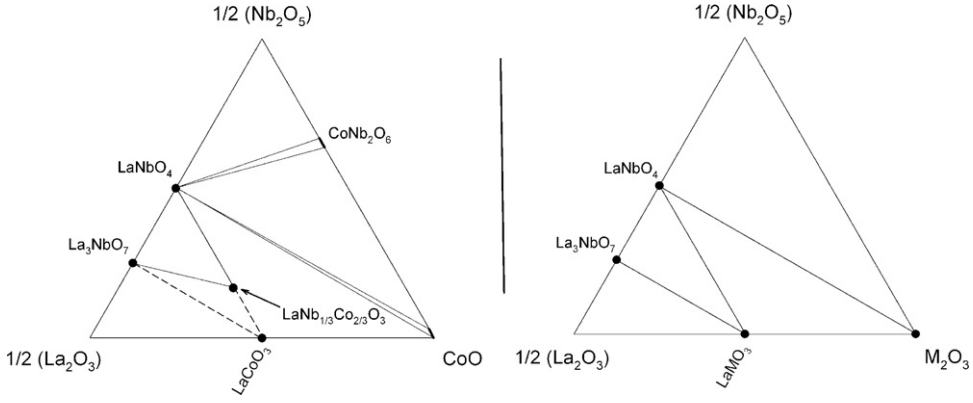

Fig. 8. Predicted phase diagrams for La_2O_3–CoO–Nb_2O_5 and La_2O_3–M_2O_3–Nb_2O_5 (M═Mn, Fe) based on this work and existing phase diagrams (see text for references).

Ruddlesden–Popper type cathode materials[23] are too La-rich and are thus unsuitable for application with $LaNbO_4$. The other two coexistent phases found for the M=Ni system, $NiNb_2O_6$ and NiO are not known as cathode materials, though the latter is often used as a precursor in the formation of electrolyte-cermet anodes. Coexistence of both NiO and Ni with $LaNbO_4$ thus simplifies the manufacture of Ni-$LaNbO_4$ cermets, allowing co-firing of cell components in air without reaction.

The formation of the $LaNb_{1/3}M_{2/3}O_3$ phases in the M=Co/Ni systems highlights the importance of pO_2 and T with respect to the systems studied here, as the relative stability of this phase with respect to $LaMO_3$ is governed by the relative stabilities of M^{2+} and M^{3+}. Accordingly, phase diagrams for the M=Mn, Fe and Co can be tentatively suggested based on the reactions of the respective $LaMO_3$ materials studied, and existing literature for the La_2O_3–M_2O_3/MO binary joins.[24–27] These are presented in Fig. 8.

For M=Co, the similarities between the NiO–Nb_2O_5 and CoO–Nb_2O_5 systems[17] extend to the La_2O_3–CoO–Nb_2O_5 ternary diagram. The significant difference is the stability of $LaCoO_3$ under ambient pO_2 and the corresponding instability of the Ruddlesden–Popper phases seen for the nickelate system,[23] resulting in coexistence of La_3NbO_7 and $LaCoO_3$ in air. Of particular interest is the stability of both the reduced $LaNb_{1/3}Co_{2/3}O_3$ (Co^{2+}) and the oxidised $LaCoO_3$ (Co^{3+}) in air, as it suggests that the former of these is entropy stabilised. Consequently this phase, and any solid solubility between the structurally similar $LaCoO_3$, should be very sensitive to changes in both T and pO_2. The improved stability of M^{3+} for M=Mn and Fe implies a much broader pO_2–T window for coexistence with $LaNbO_4$, with formation of the $LaNb_{1/3}M_{2/3}O_3$ phases unlikely except under strongly reducing conditions. An additional variable arises due to the non-stoichiometry observed for $LaMnO_3$, linked to the formation of Mn^{4+},[28] and accordingly a small solid solution region exists around this composition.[26] With increasing pO_2 the formation of Mn^{4+} can thus not be ignored, though it is unlikely alter the phase relations given here.

Available thermal expansion data for the systems investigated here is presented in Table 3, and it is clear that whilst the perovskite materials represent a favourable chemical match with $LaNbO_4$, thermophysical compatibility is more complex. The most obvious challenge is the marked change in TEC above and below the monoclinic–tetragonal phase transition, with anisotropic expansion characteristics, particularly for the low temperature phase,[29] complicating this further. It is therefore perhaps surprising that whilst the $LaMnO_3$ couple shows poor connectivity (Fig. 2), the $LaFeO_3$ phase remains well connected to the $LaNbO_4$ (Fig. 3). This can be understood in terms of the *relative* expansion coefficients of these materials: The TEC for the perovskite materials lie between the TEC's for the two polymorphs of $LaNbO_4$, so at high temperatures (where the samples are sintered), the relatively higher TEC of the perovskite phase generates tensile stress on cooling. However, below the $LaNbO_4$ phase transition the difference in the relative expansions of the two phases reverses so that cooling below the transition then acts to relieve the accumulated stress. The challenge is thus to form the $LaMO_3$/$LaNbO_4$ interface such that stresses in the high temperature region can be accommodated without interfacial cracking and separation. As the $LaMO_3$ perovskites tend to show similar TEC's (excepting the $LaCoO_3$ family), control of interfacial microstructure thus becomes critical, with compositions showing high fracture strength being favoured.

Table 3
Linear thermal expansion coefficients for the compositions used in this study.

Composition	Temperature range	TEC (K-1)	Reference
$LaNbO_4$	473–773 K	14×10^{-6}	35
	800–973 K	8.4×10^{-6}	
$LaMnO_3$	1123 K	11.33×10^{-6}	36
$LaFeO_3$	573–693 K	11.6×10^{-6}	37
	753–1193 K	10.9×10^{-6}	
$LaCoO_3$	RT–1100 K	$20–22 \times 10^{-6}$	38
$LaCr_{0.4}Ni_{0.6}O_3$	385–1323 K	10.6×10^{-6}	39

5. Conclusions

The solid-state reaction of $LaNbO_4$ with $LaMO_3$ M=Mn, Fe, Co and with La_2NiO_4 has been evaluated and representative phase diagrams for the systems proposed. $LaNbO_4$ shows general coexistence with perovskite-type compositions and transition metal binary oxides, but not with Ruddlesden–Popper type ($A_{n+1}B_nO_{3n+1}$) type phases. The $LaFeO_3$ and $LaMnO_3$ systems show no reaction with $LaNbO_4$. Coexistence of $LaNbO_4$ with both NiO and Ni has been directly confirmed, suggesting the possibility of a simple and direct route for the manufacture of $LaNbO_4$ based electrochemical cells using doped $LaMO_3$ (M=Mn, Fe) and Ni-$LaNbO_4$ cermet electrodes. Challenging thermal expansion characteristics for $LaNbO_4$ do complicate the matching of partner materials, but it is predicted that good connectivity between cell components can be achieved via careful materials choice coupled with control of interfacial microstructure.

Additionally, two new perovskite-type phases of composition $LaNb_{1/3}M_{2/3}O_3$ (M=Ni, Co) have been identified, taking an analogous structure to that of $LaNb_{1/3}Mg_{2/3}O_3$. The composition $LaNb_{1/3}Co_{2/3}O_3$ appears to be entropy stabilised, suggesting that stability of both may be strongly sensitive to pO_2 and temperature.

Acknowledgments

The authors would express their thanks to Rune Barland, Øystein Anderson and Trine Øyås for powder preparation. Funding for this work was provided by the NANOMAT programme; grant no. 158517413 – "Functional Oxides for Energy Technology".

References

1. Iwahara, H., Proton conducting ceramics and their applications. *Solid State Ionics*, 1996, **86**(8), 9–15.
2. Bohn, H. G. and Schober, T., Electrical conductivity of the high-temperature proton conductor $BaZr_{0.9}Y_{0.1}O_{2.95}$. *J. Am. Ceram. Soc.*, 2000, **83**, 768–772.

3. Yajima, T. and Iwahara, H., Studies on proton behavior in doped perovskite-type oxides. II. Dependence of equilibrium hydrogen concentration and mobility on dopant content in Yb-doped $SrCeO_3$. *Solid State Ionics*, 1992, **53–56**, 983–988.
4. Kreuer, K. D., Proton-conducting oxides. *Ann. Rev. Mater. Res.*, 2003, **33**, 333–359.
5. Iwahara, H., Technological challenges in the application of proton conducting ceramics. *Solid State Ionics*, 1995, **77**, 289–298.
6. Scholten, M. J., Schoonman, J., Vanmiltenburg, J. C. and Oonk, H. A. J., Synthesis of strontium and barium cerate and their reaction with carbon dioxide. *Solid State Ionics*, 1993, **61**, 83–91.
7. Anselmi-Tamburini, U., Buscaglia, M. T., Viviani, M., Bassoli, A., Bottino, C., Buscaglia, V. *et al.*, Solid-state synthesis and spark plasma sintering of submicron $BaY_xZr_{1-x}O_{3-x/2}$ ($x = 0$, 0.08 and 0.16) ceramics. *J. Eur. Ceram. Soc.*, 2006, **26**, 2313–2318.
8. Haugsrud, R. and Norby, T., Proton conduction in rare-earth ortho-niobates and ortho-tantalates. *Nat. Mater.*, 2006, **5**, 193–196.
9. Haugsrud, R. and Norby, T., High-temperature proton conductivity in acceptor-doped $LaNbO_4$. *Solid State Ionics*, 2006, **177**, 1129–1135.
10. Fukada, S., Suemori, S. and Onoda, K., Proton transfer in $SrCeO_3$-based oxide with internal reformation under supply of CH_4 and H_2O. *J. Nucl. Mater.*, 2006, **348**, 26–32.
11. Song, S. J., Lee, T. H., Wachsman, E. D., Chen, L., Dorris, S. E. and Balachandran, U., Defect structure and transport properties of Ni–$SrCeO_3$–delta cermet for hydrogen separation membrane. *J. Electrochem. Soc.*, 2005, **152**, J125–J129.
12. Iwahara, H., Asakura, Y., Katahira, K. and Tanaka, M., Prospect of hydrogen technology using proton-conducting ceramics. *Solid State Ionics*, 2004, **168**, 299–310.
13. Boehm, E. and McEvoy, A. J., Protonic electroceramics for fuel cells. *Fuel Cells*, 2006, **6**, 54–58.
14. Mokkelbost, T., Andersen, Ø., Strom, R. A., Wiik, K., Grande, T. and Einarsrud, M.-A., High temperature proton conducting $LaNbO_4$-based materials. Part II. Sintering properties and solubility of alkali earth oxides. *J. Am. Ceram. Soc.*, 2007, **90**, 3395–3433.
15. Choi, I. K., Cho, B. J., Paik, J. H., Nahm, S., Kim, J. S., Lee, H. J. *et al.*, Crystal structure of $La(Mg_{2/3}Nb_{1/3})O_3$ ceramics. *Mater. Res. Bull.*, 2000, **35**, 921–928.
16. JCPDS-ICDD database, 1999.
17. Burdese, A., Borlera, M. L. and Rolando, P., Systems between niobium and the oxides of nickel and cobalt. *Atti Accad. Sci. Torino: I. Classe Sci. Fis. Mater. Nat.*, 1964–1965, **99**, 565–575.
18. Zinkevich, M. and Aldinger, F., Thermodynamic analysis of the ternary La–Ni–O system. *J. Alloys Compd.*, 2004, **375**, 147–161.
19. Zuev, M. G., Phase behavior of in the systems La_2O_3–B_2O_3–Ta_2O_5 and La_2O_3–B_2O_3–Nb_2O_5 in the subsolidus region. *Zhur. Neorganicheskoi Khim.*, 1998, **43**, 1229–1232.
20. Zhang, Z. and Greenblatt, M., Synthesis, structure, and properties of $Ln_4Ni_3O_{10-\delta}$ (Ln = La, Pr, and Nd). *J. Solid State Chem.*, 1995, **117**, 236–246.
21. Khamman, O., Yimnirun, R. and Ananta, S., Phase and morphology evolution of corundum-type $Ni_4M_2O_9$ powders synthesized by solid-state reaction. *Mater. Lett.*, 2007, **61**, 2565–2570.
22. Bogatskii, D. P., State diagram of the system nickel-oxygen and physicochemical nature of the solid phases in that system. *Zhurnal Obshchei Khimii*, 1951, **21**, 3–10.
23. Amow, G., Davidson, I. J. and Skinner, S. J., A comparative study of the Ruddlesden–Popper series, $La_{n+1}Ni_nO_{3n+1}$ ($n = 1$, 2 and 3), for solid-oxide fuel-cell cathode applications. *Solid State Ionics*, 2006, **177**, 1205–1210.
24. Fossdal, A., Einarsrud, M.-A. and Grande, T., Phase relations in the pseudo ternary system La_2O_3–SrO–Fe_2O_3. *J. Am. Ceram. Soc.*, 2005, **88**, 1988.
25. Grundy, A. N., Hallstedt, B. and Gauckler, L. J., *Calphad*, 2004, **28**, 191.
26. Vanroosmalen, J. A. M., Vanvlaanderen, P., Cordfunke, E. H. P., Ijdo, W. L. and Ijdo, D. J. W., Phases in the perovskite-type $LaMnO_{3+\delta}$ solid solution and the La_2O_3–Mn_2O_3 phase diagram. *J. Solid State Chem.*, 1995, **114**, 516–523.
27. Kitayama, K., Thermogravimetric study of the Ln_2O_3–Co–Co_2O_3 system. *J. Solid State Chem.*, 1997, **131**, 18–23.
28. Bakken, E., Norby, T. and Stolen, S., Redox energetics of perovskite-related oxides. *J. Mater. Chem.*, 2002, **12**, 317–323.
29. Jian, L. and Wayman, C. M., Monoclinic-to-tetragonal phase transformation in a ceramic rare-earth orthoniobate, $LaNbO_4$. *J. Am. Ceram. Soc.*, 1997, **80**, 803–806.
30. Cheetham, A. K., Rao, C. N. R. and Vogt, T., Magnetic structure and giant magnetoresistance of ferromagnetic $La_{1-\delta}Mn_{1-\delta}O_3$—An example of double-exchange striction? *J. Solid State Chem.*, 1996, **126**, 337–341.
31. Tsunekawa, S., Kamiyama, T., Sasaki, K., Asano, H. and Fukuda, T., Precise structure-analysis by neutron-diffraction for $RNbO_4$ and distortion of NbO_4 tetrahedra. *Acta Cryst. A*, 1993, **49**, 595–600.
32. Falcon, H., Goeta, A. E., Punte, G. and Carbonio, R. E., Crystal structure refinement and stability of $LaFe_xNi_{1-x}O_3$ solid solutions. *J. Solid State Chem.*, 1997, **133**, 379–385.
33. Jorgensen, J. D., Dabrowski, B., Pei, S., Richards, D. R. and Hinks, D. G., Structure of the interstitial oxygen defect in $La_2NiO_{4+\delta}$. *Phys. Rev. B*, 1989, **40**, 2187–2199.
34. Kahn-harari, A., Mazerolles, L., Michel, D. and Robert, F., Structural description of La_3NbO_7. *J. Solid State Chem.*, 1995, **116**, 103–106.
35. Mokkelbost, T., Lein, H. L., Vullum, P. E., Holmestad, R., Grande, T. and Einarsrud, M.-A., High temperature proton conducting $LaNbO_4$-based materials. Part III. Mechanical and thermal properties. *Ceram. Int.*, in press.
36. Raj, E. S., Skinner, S. J. and Kilner, J. A., Solution synthesis and electrical properties of K_2NiF_4 type $LaSrAlO_4$. *Solid State Sci.*, 2004, **6**, 825–829.
37. Fossdal, A., Menon, M., Waernhus, I., Wiik, K., Einarsrud, M. A. and Grande, T., Crystal structure and thermal expansion of $La_{1-x}Sr_xFeO_{3-\delta}$ materials. *J. Am. Ceram. Soc.*, 2004, **87**, 1952–1958.
38. Kharton, V. V., Naumovich, E. N., Kovalevsky, A. V., Viskup, A. P., Figueiredo, F. M., Bashmakov, I. A. *et al.*, Mixed electronic and ionic conductivity of $LaCo(M)O_3$ (M=Ga, Cr, Fe or Ni). IV. Effect of preparation method on oxygen transport in $LaCoO_{3-\delta}$. *Solid State Ionics*, 2000, **138**, 135–148.
39. Hofer, H. E. and Kock, W. F., Crystal-chemistry and thermal-behaviour in the $La(CrNi)O_3$ perovskite system. *J. Electrochem. Soc.*, 1993, **140**, 2889–2894.